Complete temporal mode analysis in pulse-pumped fiber-optical parametric amplifier for continuous variable entanglement generation

Xueshi Guo,[1] **Nannan Liu,**[1] **Xiaoying Li,**[1,*] **Z. Y. Ou**[2]

[1]*College of Precision Instrument and Opto-electronics Engineering, Tianjin University, Key Laboratory of Optoelectronics Information Technology of Ministry of Education, Tianjin 300072, China*

[2]*Department of Physics, Indiana University-Purdue University Indianapolis, Indianapolis, IN 46202, USA*

[*]*xiaoyingli@tju.edu.cn*

Abstract: Mode matching plays an important role in measuring the continuous variable entanglement. For the signal and idler twin beams generated by a pulse pumped fiber optical parametric amplifier (FOPA), the spatial mode matching is automatically achieved in single mode fiber, but the temporal mode property is complicated because it is highly sensitive to the dispersion and the gain of the FOPA. We study the temporal mode structure and derive the input-output relation for each temporal mode of signal and idler beams after decomposing the joint spectral function of twin beams with the singular-value decomposition method. We analyze the measurement of the quadrature-amplitude entanglement, and find mode matching between the multi-mode twin beams and the local oscillators of homodyne detection systems is crucial to achieve a high degree of entanglement. The results show that the noise contributed by the temporal modes nonorthogonal to local oscillator may be much larger than the vacuum noise, so the mode mis-match can not be accounted for by merely introducing an effective loss. Our study will be useful for developing a source of high quality continuous variable entanglement by using the FOPA.

OCIS codes: (270.0270) Quantum optics; (190.4380) Nonlinear optics, four-wave mixing; (320.7140) Ultrafast processes in fibers.

References and links

1. M. D. Reid, P. D. Drummond, W. P. Bowen, E. G. Cavalcanti, P. K. Lam, H. A. Bachor, U. L. Andersen, and G. Leuchs, "Colloquium: the einstein-podolsky-rosen paradox: from concepts to applications," Rev. Mod. Phys. **81**, 1727–1751 (2009).
2. L. S. Madsen, V. C. Usenko, M. Lassen, R. Filip, and U. L. Andersen, "Continuous variable quantum key distribution with modulated entangled states," Nat. Commun. **3**, 1083 (2012).
3. C. Silberhorn, N. Korolkova, and G. Leuchs, "Quantum key distribution with bright entangled beams," Phys. Rev. Lett. **88**, 167902 (2002).
4. V. Boyer, A. M. Marino, R. C. Pooser, and P. D. Lett, "Entangled images from four-wave mixing," Science **321**, 544–547 (2008).
5. Z. Y. Ou, S. F. Pereira, H. J. Kimble, and K. C. Peng, "Realization of the einstein-podolsky-rosen paradox for continuous variables," Phys. Rev. Lett. **68**, 3663–3666 (1992).

#250441 Received 18 Sep 2015; accepted 27 Oct 2015; published 2 Nov 2015

6. V. Josse, A. Dantan, A. Bramati, M. Pinard, and E. Giacobino, "Continuous variable entanglement using cold atoms," Phys. Rev. Lett. **92**, 123601 (2004).
7. A. M. Marino, R. C. Pooser, V. Boyer, and P. D. Lett, "Tunable delay of einstein-podolsky-rosen entanglement," Nature **457**, 859–862 (2009).
8. E. Flurin, N. Roch, F. Mallet, M. H. Devoret, and B. Huard, "Generating entangled microwave radiation over two transmission lines," Phys. Rev. Lett. **109**, 183901 (2012).
9. C. Silberhorn, P. K. Lam, O. Weiß, F. König, N. Korolkova, and G. Leuchs, "Generation of continuous variable einstein-podolsky-rosen entanglement via the kerr nonlinearity in an optical fiber," Phys. Rev. Lett. **86**, 4267–4270 (2001).
10. T. Eberle, V. Händchen, J. Duhme, T. Franz, R. F. Werner, and R. Schnabel, "Strong Einstein-Podolsky-Rosen entanglement from a single squeezed light source," Phys. Rev. A **83**, 052329 (2011).
11. G. P. Agrawal, "Nonlinear fiber optics" (Academic Press, 2007).
12. M. Fiorentino, P. L. Voss, J. E. Sharping, and P. Kumar, "All-fiber photon-pair source for quantum communications," Photonics Technol. Lett. **14**, 983–985 (2002).
13. L. Yang, X. Ma, X. Guo, L. Cui, and X. Li, "Characterization of a fiber-based source of heralded single photons," Phys. Rev. A **83**, 053843 (2011).
14. J. E. Sharping, M. Fiorentino, and P. Kumar, "Observation of twin-beam-type quantum correlation in optical fiber," Opt. Lett. **26**, 367–369 (2001).
15. X. Guo, X. Li, N. Liu, L. Yang, and Z. Y. Ou, "An all-fiber source of pulsed twin beams for quantum communication," Appl. Phys. Lett. **101**, 261111–261115 (2012).
16. X. Guo, X. Li, N. Liu, and Y. Liu, "Generation and characterization of continuous variable quantum correlations using a fiber optical parametric amplifier," in *Conference on Lssers and Electro Optics* (OSA, 2015), p. JW2A.6
17. R. M. Shelby, M. D. Levenson, and P. W. Bayer, "Guided acoustic-wave brillouin scattering," Phys. Rev. B, **31**, 5244 (1985).
18. P. L. Voss, K. G. Koprulu, and P. Kumar, "Raman-noise-induced quantum limits for $\chi^{(3)}$ nondegenerate phase-sensitive amplification and quadrature squeezing," J. Opt. Soc. Am. B, **23**, 598–610 (2006).
19. Z. Y. Ou, "Parametric down-conversion with coherent pulse pumping and quantum interference between independent fields," Quantum Semiclass. Opt. **9**, 599 (1997).
20. W. Wasilewski, A. I. Lvovsky, K. Banaszek, and C. Radzewicz, "Pulsed squeezed light: Simultaneous squeezing of multiple modes," Phys. Rev. A **73**, 063819 (2006).
21. C. J. McKinstrie, S. J. van Enk, M. G. Raymer, and S. Radic, "Multicolor multipartite entanglementproduced by vector four-wave mixingin a fiber," Opt. Express **16**, 2720–2739 (2008).
22. X. Guo, X. Li, N. Liu, and Z. Y. Ou, "Multimode theory of pulsed-twin-beam generation using a high-gain fiber-optical parametric amplifier," Phys. Rev. A **88**, 023841 (2013).
23. P. J. Mosley, J. S. Lundeen, B. J Smith, P. Wasylczyk, A. B. U'Ren, C. Ciberhorn, and I. A Walmsley, "Heralded generation of ultrafast single photons in pure quantum states," Phys. Rev. Lett. **100**, 133601 (2008).
24. A. Eckstein, A. Christ, P. J. Mosley, and C. Silberhorn, "Highly efficient single-pass source of pulsed single-mode twin beams of light," Phys. Rev. Lett. **106**, 013603 (2011).
25. J. E. Gentle, *Numerical Linear Algebra for Applications in Statistics* (Springer-Verlag, 1998).
26. X. Li, X. Ma, Z. Y. Ou, L. Yang, L. Cui, and D. Yu, "Spectral study of photon pairs generated in dispersion shifted fiber with a pulsed pump," Opt. Express **16**, 32–44 (2008).
27. L.-M. Duan, G. Giedke, J. I. Cirac, and P. Zoller, "Inseparability criterion for continuous variable systems," Phys. Rev. Lett. **84**, 2722–2725 (2000).
28. S. L. Braunstein and D. D. Crouch, "Fundamental limits to observations of squeezing via balanced homodyne detection," Phys. Rev. A **43**, 330–337 (1991).
29. Yoon-Ho Kim, and Warren P. Grice, "Measurement of the spectral properties of the two-photon state generated via Type II spontaneous parametric downconversion," Opt. Lett. **30**, 908 (2005).
30. W. Wasilewski, P. Wasylczyk, P. Kolenderski, K. Banaszek, and C. Radzewicz, "Joint spectrum of photon pairs measured by coincidence Fourier spectroscopy," Opt. Lett. **31**, 1130 (2006).
31. A. Eckstein, G. Boucher, A. Lemaître, P. Filloux, I. Favero, G. Leo, J. E. Sipe, M. Liscidini, and S. Ducci, "High-resolution spectral characterization of two photon states via classical measurements," Laser Photonics Rev. **8**, L76–L80 (2014).
32. M. Liscidini and J. E. Sipe, "Stimulated emission tomography," Phys. Rev. Lett. **111**, 193602 (2013).
33. C. Polycarpou, K. N. Cassemiro, G. Venturi, A. Zavatta, and M. Bellini, "Adaptive detection of arbitrarily shaped ultrashort quantum light states," Phys. Rev. Lett. **109**, 053602 (2012).

1. Introduction

Continuous variable (CV) entanglement, whose quadrature-phase amplitudes possess quantum correlation, is not only an important non-classical light source for studying quantum effects, but also a powerful resource for quantum information technologies, such as quantum metrology and

#250441 Received 18 Sep 2015; accepted 27 Oct 2015; published 2 Nov 2015

quantum imaging [1–4]. Quadrature-amplitude entangled optical fields at different wavelength have been successfully generated by invoking non-degenerate parametric process in a variety of nonlinear media [5–8], or by coherently combining two quadrature-amplitude squeezed states at beam splitters [9, 10]. Nevertheless, constructing a high quality and compact source of CV entanglement is still currently quite challenging.

Fiber-optical parametric amplifiers (FOPA), based on the four-wave mixing (FWM) in optical fibers, provide a convenient and powerful tool to realize optical amplification in broadband and flexible wavelength range. On the one hand, all-optical functional operations, such as wavelength conversion, phase-conjugate wave generation, and ultrahigh speed switching, can be realized by utilizing FWM in fibers [11]. On the other hand, FOPA is also a prominent device to generate non-classical lights. Indeed, a variety of quantum states, such as entangled photon pairs, single photons, and twin beams with intensity difference squeezing, have been generated by FOPAs [12–15]. However, the generation of CV entanglement via an FOPA is less studied [16]. This is partly because, for a FOPA based quantum light source, one usually uses pulsed pump to suppress the background noise, such as guided acoustic wave Brillouin scattering (GAWBS) and Raman scattering [17, 18]. As a result, the temporal mode structure of pulse-pumped FOPAs is much more complicated than those pumped with continuous wave (CW) light [19,20]. A relatively thorough theoretical analysis on the generation of CV entanglement via a CW laser pumped FOPA was presented in Ref. [21], but the complexity of temporal mode is not considered. In our previous work [22], we attempted to provide a theoretical model of a pulsed pumped FOPA to analyze the intensity difference squeezing of the twin beams, but the heavy numerical simulations had to be carried out due to the mathematical complexity.

The major complexity involved in the pulse-pumped parametric process is the complicated frequency correlation between the signal and idler twin beams [19]. This leads to mixed intermode coupling in frequency domain [22] and thus the mode mismatch between the pulsed local oscillator and signal/idler fields when homodyne detection is utilized for measuring the quadrature components. The effect of mode mismatch in homodyne detection is usually modeled by an effective loss, which introduces the vacuum noise and hence reduces the degree of quantum entanglement of twin beams. It was argued that a factorized joint spectral function of the signal and idler fields is necessary to decouple the frequency correlation and to describe the process in a single temporal mode fashion [23,24]. Recently, Wasilewski et al. utilize the singular value decomposition (SVD) to decompose the fields generated from a pulse-pumped parametric amplifier into orthogonal temporal modes [20], which leads to decoupling of the modes. However, the decomposition is on the Green functions that are related to the interaction Hamiltonian in a complicated manner. Therefore, the mode analysis has to resort to numerical methods and does not seem to provide useful insight for the experimental investigation. Nevertheless, the decoupling of the temporal modes significantly simplifies the discussions on the quantum nature (noise reduction) of the signal and idler fields.

In this paper, we follow the same idea of Wasilewski et al [20] for mode decomposition. However, instead of decomposing the Green functions, we apply the SVD method to the so called joint spectral function (JSF) that is directly related to the interaction Hamiltonian and can be directly determined by the experimental parameters of pump and nonlinear medium. We first extend our multi-frequency model in Ref. [22] and derive the evolution of the decomposed temporal modes, showing that the temporal modes are completely decoupled. We then theoretically study the CV entanglement properties of the twin beams by numerically calculating the degree of entanglement when the experimental parameters of the FOPA and the local oscillators are varied. The result shows that the influence of the temporal mode mismatch on the homodyne detection process are far more complicated than the simple model of an effective detection loss due to the coherent superposition of the temporal modes of twin beams. Therefore,

#250441 Received 18 Sep 2015; accepted 27 Oct 2015; published 2 Nov 2015

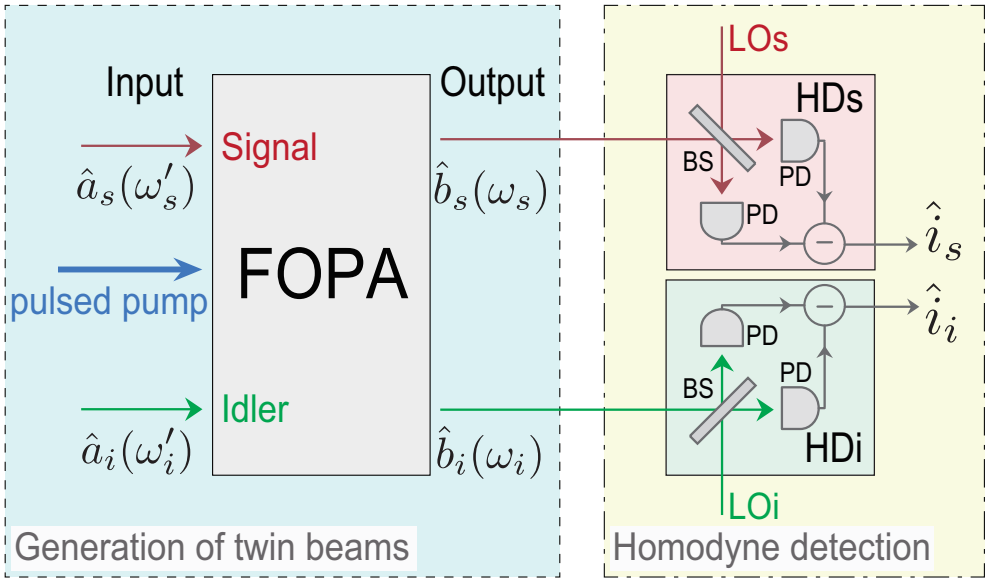

Fig. 1. Conceptual diagram of generating quadrature amplitude entanglement from a fiber optical parametric amplifier (FOPA). $\hat{a}_{s(i)}(\omega'_{s(i)})$, the operator of input signal (idler) field; $\hat{b}_{s(i)}(\omega_{s(i)})$, the operator of the output signal (idler) field; HDs/HDi, homodyne detection system for signal/idler field; LOs/LOi: Local oscillators of HDs/HDi; $\hat{i}_{s(i)}$: the operator of photocurrent out of HDs/HDi.

controlling the mode-matching between the temporal modes of the signal/idler beam and the local oscillator of homodyne detection systems is crucial for developing a high quality source of pulsed CV entanglement.

The rest of the paper is organized as follows: In Sec. II, after briefly reviewing our previous work [22] on the evolution of the output fields generated from a pulse-pumped FOPA, we characterize the temporal mode structure of the signal and idler fields after applying the SVD to JSF and derive the input-output relation of the FOPA in each temporal mode. In Sec. III, we analyze the entanglement properties of signal and idler beams in the decomposed temporal modes. In Sec. IV, we discuss the influence of mode matching when the quadrature entanglement is measured by the homodyne detection system. Finally, we briefly conclude in Sec. V.

2. Temporal mode property of the signal and idler fields generated from a pulse-pumped FOPA

2.1. *Multi-frequency mode model*

We start by introducing the multi-frequency mode theory developed in Ref. [22]. For the parametric process of four wave mixing (FWM) in a pulse pumped FOPA (see the area in dashed frame in Fig.1), two pump photons at angular frequencies ω_{p1} and ω_{p2} are coupled via $\chi^{(3)}$ of the nonlinear fiber to simultaneously create signal and idler photons at frequencies ω_s and ω_i, respectively, such that $\omega_{p1}+\omega_{p2}=\omega_s+\omega_i$. The Hamiltonian of this process is

$$\hat{H}(t)=C_1\chi^{(3)}\int dV[E_{p1}(t)E_{p2}(t)\hat{E}_s^{(-)}(t)\hat{E}_i^{(-)}(t)+h.c.], \tag{1}$$

where C_1 is a constant determined by experimental details and the units of quantized optical fields, E_{p1} and E_{p2} are the fields of strong pump pulses propagating along the fiber. When the

#250441 Received 18 Sep 2015; accepted 27 Oct 2015; published 2 Nov 2015

FOPA is pumped with a transform limited pulsed laser, whose spectrum is Gaussian shaped, we have

$$E_{pn}(t) = E_0 e^{-i\gamma P_p z} \int e^{-(\omega_{pn}-\omega_{p0})^2/2\sigma_p^2} e^{i(k_p z - \omega_{pn} t)} d\omega_{pn} \quad (n = 1, 2), \tag{2}$$

where σ_p, ω_{p0} and k_p are the bandwidth, central frequency, and wave vector of the pump, respectively, and E_0 is related to the peak power through the relation $P_p = 2\pi\sigma_p^2 E_0^2$. The phase term $e^{-i\gamma P_p z}$ is originated from the self-phase modulation with $\gamma = \frac{3\omega_{p0}\chi^{(3)}}{8cA_{eff}}$ denoting the nonlinear coefficient of fiber, where A_{eff} denotes the effective mode area of fiber and c is the speed of light in vacuum. The quantized one-dimensional negative-frequency field operators

$$\hat{E}_s^{(-)}(t) = \frac{1}{\sqrt{2\pi}} \int d\omega_s' \hat{a}_s^\dagger(\omega_s') e^{-i(k_s z - \omega_s' t)} \tag{3a}$$

and

$$\hat{E}_i^{(-)}(t) = \frac{1}{\sqrt{2\pi}} \int d\omega_i' \hat{a}_i^\dagger(\omega_i') e^{-i(k_i z - \omega_i' t)} \tag{3b}$$

respectively describe the inputs of signal and the idler fields. After substituting Eqs. (2) and (3) into Eq. (1) and changing dV in Eq. (1) to $dV = A_{eff} dz$, we carry out the integral over the whole fiber length L (from 0 to L) and arrive at the Hamiltonian in the time dependent form

$$\begin{aligned} \hat{H}(t) = \quad & \frac{2C_1 \gamma P_p L c A_{eff}^2}{3\omega_{p0}\pi^2\sigma_p^2} \int d\omega_{p1} d\omega_{p2} d\omega_s' d\omega_i' \hat{a}_s^\dagger(\omega_s') \hat{a}_i^\dagger(\omega_i') \\ & \operatorname{sinc}\left(\frac{\Delta k L}{2}\right) \exp\left\{ -\frac{(\omega_{p1}-\omega_{p0})^2 + (\omega_{p2}-\omega_{p0})^2}{2\sigma_p^2} \right\} e^{-i(\omega_{p1}+\omega_{p2}-\omega_s'-\omega_i')t} + h.c. \end{aligned} \tag{4}$$

where $\Delta k = k_s + k_i - 2k_p + 2\gamma P_p$ with $k_{s(i)}$ denoting the wave vector of signal (idler) field is the phase mismatching term.

Because of the broadband nature of the pulsed pump fields, the output signal (idler) field $\hat{b}_{s(i)}(\omega_{s(i)})$ is a superposition of many amplified input signal (idler) frequency modes $\hat{a}_{s(i)}(\omega_{s(i)})$, and a general input-output relationships of the operators are [22]

$$\hat{b}_s(\omega_s) = \hat{U}^\dagger \hat{a}_s(\omega_s) \hat{U} = \int_S h_{1s}(\omega_s, \omega_s') \hat{a}_s(\omega_s') d\omega_s' + \int_I h_{2s}(\omega_s, \omega_i') \hat{a}_i^\dagger(\omega_i') d\omega_i' \tag{5a}$$

$$\hat{b}_i(\omega_i) = \hat{U}^\dagger \hat{a}_i(\omega_i) \hat{U} = \int_I h_{1i}(\omega_i, \omega_i') \hat{a}_i(\omega_i') d\omega_i' + \int_S h_{2i}(\omega_i, \omega_s') \hat{a}_s^\dagger(\omega_s') d\omega_s', \tag{5b}$$

where S and I respectively represent the integration frequency range of the signal and idler fields, and the functions $h_{1s}, h_{2s}, h_{1i}, h_{2i}$ are referred to as Green functions, which determine the amplification process of FOPA. The operators of the input and output fields satisfy the commutation relation $[\hat{a}_s(\omega_{s1}'), \hat{a}_s^\dagger(\omega_{s2}')] = \delta(\omega_{s1}' - \omega_{s2}')$ and $[\hat{b}_s(\omega_{s1}), \hat{b}_s^\dagger(\omega_{s2})] = \delta(\omega_{s1} - \omega_{s2})$, respectively. The unitary evolution operator

$$\hat{U} = \exp\left\{ \frac{\int \hat{H}(t) dt}{i\hbar} \right\} = \exp\left\{ G\left[\iint F(\omega_s', \omega_i') \hat{a}_s^\dagger(\omega_s') \hat{a}_i^\dagger(\omega_i') d\omega_s' d\omega_i' - h.c. \right] \right\}, \tag{6}$$

is determined by the Hamiltonian in Eq. (4), where $G \propto \gamma P_p L$ is the gain coefficient of FWM, and the joint spectrum function (JSF)

$$F(\omega_s', \omega_i') = C_N \exp\left(\frac{-i\Delta k L}{2}\right) \exp\left\{ \frac{-(\omega_s' + \omega_i' - 2\omega_{p0})^2}{4\sigma_p^2} \right\} \operatorname{sinc}\left(\frac{\Delta \mathrm{k} \mathrm{L}}{2}\right), \tag{7}$$

#250441 Received 18 Sep 2015; accepted 27 Oct 2015; published 2 Nov 2015

with C_N denoting a constant to ensure the satisfaction of normalization condition $\iint |F(\omega_s', \omega_i')|^2 d\omega_s' d\omega_i' = 1$, is referred to as the probability amplitude of simultaneously finding a pair of signal and idler photons within the frequency range of $\omega_s' \to \omega_s' + d\omega_s'$ and $\omega_i' \to \omega_i' + d\omega_i'$, respectively.

According to Ref. [22], the Green functions in Eq.(5) are related to the JSF $F(\omega_s, \omega_i)$ and the gain coefficient G in the form of an infinite series

$$\begin{aligned} h_{1s}(\omega_s, \omega_s') = \quad & \delta(\omega_s - \omega_s') + \sum_{n=1}^{\infty} \frac{G^{2n}}{(2n)!} \iint \cdots \int d\omega_1 d\omega_2 \cdots d\omega_{2n-1} \\ \{ \quad & F(\omega_s, \omega_1) F(\omega_2, \omega_3) F(\omega_4, \omega_5) \cdots F(\omega_{2n-2}, \omega_{2n-1}) \times \\ & F^*(\omega_2, \omega_1) F^*(\omega_4, \omega_3) F^*(\omega_6, \omega_5) \cdots F^*(\omega_s', \omega_{2n-1}) \} \end{aligned} \tag{8}$$

$$\begin{aligned} h_{2s}(\omega_s, \omega_i') = \quad & GF(\omega_s, \omega_i') + \sum_{n=1}^{\infty} \frac{G^{2n+1}}{(2n+1)!} \iint \cdots \int d\omega_1 d\omega_2 \cdots d\omega_{2n} \\ \{ \quad & F^*(\omega_2, \omega_1) F^*(\omega_4, \omega_3) \cdots F^*(\omega_{2n}, \omega_{2n-1}) \times \\ & F(\omega_s, \omega_1) F(\omega_2, \omega_3) F(\omega_4, \omega_5) \cdots F(\omega_{2n}, \omega_i') \} \end{aligned} \tag{9}$$

$$\begin{aligned} h_{1i}(\omega_i, \omega_i') = \quad & \delta(\omega_i - \omega_i') + \sum_{n=1}^{\infty} \frac{G^{2n}}{(2n)!} \iint \cdots \int d\omega_1 d\omega_2 \cdots d\omega_{2n-1} \\ & \{ F(\omega_1, \omega_i) F(\omega_3, \omega_2) F(\omega_5, \omega_4) \cdots F(\omega_{2n-1}, \omega_{2n-2}) \times \\ & F^*(\omega_1, \omega_2) F^*(\omega_3, \omega_4) F^*(\omega_5, \omega_6) \cdots F^*(\omega_{2n-1}, \omega_i') \} \end{aligned} \tag{10}$$

$$\begin{aligned} h_{2i}(\omega_i, \omega_s') = \quad & G\psi(\omega_s', \omega_i) + \sum_{n=1}^{\infty} \frac{G^{2n+1}}{(2n+1)!} \iint \cdots \int d\omega_1 d\omega_2 \cdots d\omega_{2n} \\ \{ \quad & F^*(\omega_1, \omega_2) F^*(\omega_3, \omega_4) \cdots F^*(\omega_{2n-1}, \omega_{2n}) \times \\ & F(\omega_1, \omega_i) F(\omega_3, \omega_2) \psi(\omega_5, \omega_4) \cdots F(\omega_s', \omega_{2n}) \} \ . \end{aligned} \tag{11}$$

2.2. *Singular value decomposition and multi-temporal mode model*

When the JSF is factorizable, i.e., $F(\omega_s, \omega_i) = \phi(\omega_s)\psi(\omega_i)$, the Green functions in Eqs. (8-11) can be significantly simplified since the signal and the idler fields can be described by a single temporal mode model [22]. In general, however, the JSF is not factorizable. In this case, after applying SVD method to JSF, we arrive at [25]

$$F(\omega_s, \omega_i) = \sum_k r_k \phi_k(\omega_s) \psi_k(\omega_i) \qquad \big(k = 1, 2, ...\big), \tag{12}$$

where the complex functions $\phi_k(\omega_s)$ and $\psi_k(\omega_i)$, satisfying the orthogonal conditions $\phi_{k1}^*(\omega_s)\phi_{k2}(\omega_s)d\omega_s = \delta_{k1,k2}$ and $\int \psi_{k1}^*(\omega_i)\psi_{k2}(\omega_i)d\omega_i = \delta_{k1,k2}$, respectively, represent the spectrum of signal and idler fields in the kth order temporal mode, and the real eigenvalue $r_k \geq 0$, satisfying the normalization condition $\sum_k |r_k|^2 = 1$, is referred to as the mode amplitude. For the sake of clarity, the mode index k are arranged in a descending order, so that the mode amplitudes satisfy $r_{k-1} \geq r_k \geq r_{k+1} \cdots$ for $k \geq 2$. For the case of $k = 1$, the functions $\phi_1(\omega_s)$ and $\psi_1(\omega_i)$ are referred to as the fundamental mode.

#250441 Received 18 Sep 2015; accepted 27 Oct 2015; published 2 Nov 2015

Substituting Eq. (12) into Eqs. (8)-(11), we can significantly simplify the Green function in the form of decomposed mode:

$$h_{1s}(\omega_s,\omega_s') = \delta(\omega_s-\omega_s')+\sum_k[\cosh(r_k\times G)-1]\phi_k(\omega_s)\phi_k^*(\omega_s') \tag{13}$$

$$h_{2s}(\omega_s,\omega_i') = \sum_k \sinh(r_k\times G)\phi_k(\omega_s)\psi_k(\omega_i') \tag{14}$$

$$h_{1i}(\omega_i,\omega_i') = \delta(\omega_i-\omega_i')+\sum_k[\cosh(r_k\times G)-1]\psi_k(\omega_i)\psi_k^*(\omega_i') \tag{15}$$

$$h_{2i}(\omega_i,\omega_s') = \sum_k \sinh(r_k\times G)\psi_k(\omega_i)\phi_k(\omega_s'). \tag{16}$$

Accordingly, the input-output relation of the FOPA in Eq. (5) can be simplified as

$$\hat{B}_{ks} = \cosh(G\times r_k)\hat{A}_{ks}+\sinh(r_k\times G)\hat{A}_{ki}^\dagger \tag{17}$$

$$\hat{B}_{ki} = \cosh(G\times r_k)\hat{A}_{ki}+\sinh(r_k\times G)\hat{A}_{ks}^\dagger, \tag{18}$$

with

$$\hat{A}_{ks} \equiv \int_S \phi_k^*(\omega_s')\hat{a}_s(\omega_s')d\omega_s' \tag{19}$$

$$\hat{A}_{ki} \equiv \int_I \psi_k^*(\omega_i')\hat{a}_i(\omega_i')d\omega_i' \tag{20}$$

$$\hat{B}_{ks} \equiv \int_S \phi_k^*(\omega_s')\hat{b}_s(\omega_s')d\omega_s' \tag{21}$$

$$\hat{B}_{ki} \equiv \int_I \psi_k^*(\omega_i')\hat{b}_i(\omega_i')d\omega_i'. \tag{22}$$

The operators in Eqs. (19)-(22) can be viewed as the generalized annihilation operators for individual SVD modes described by $\phi_k(\omega_s)$ and $\psi_k(\omega_i)$, because they always satisfy the standard commutation relationships for bosons: $[\hat{A}_{ks(ki)},\hat{A}_{ks(ki)}^\dagger]=1$ and $[\hat{B}_{ks(ki)},\hat{B}_{ks(ki)}^\dagger]=1$. In fact, the single-photon state of $\hat{A}_{ks}^\dagger|0\rangle=\int d\omega_s\phi_k(\omega_s)|1_{\omega_s}\rangle$, for example, describes a single-photon wave packet having the temporal shape of $g(t)= \quad d\omega_s\phi_k(\omega_s)e^{-i\omega_s t}/2\pi$. Notice that in Eqs. (17) and (18), different modes are decoupled from each other. The operators of signal (idler) field at the input and output of FOPA, $\hat{A}_{ks(i)}$ and $\hat{B}_{ks(i)}$, have the same temporal profile determined by $\phi_k(\omega_s)$ ($\psi_k(\omega_i)$).

2.3. *Temporal/spectral property of twin beams generated by the FOPA with broad gain bandwidth in telecom band*

Aiming at developing an all-fiber source of CV entanglement by using the commercially available fiber components, which is compact and low cost, we will analyze the temporal/spectral structure of the twin beams generated by a pulse-pumped FOPA in telecom band. We assume the central wavelength of pump is very close to the zero dispersion wavelength of the nonlinear fiber and the gain bandwidth of FWM in the fiber is very broad. In this case, for the sake of convenience, we rewrite Eq. (7) as

$$F(\Omega_s,\Omega_i)=C_N\exp\left(\frac{-i\Delta kL}{2}\right)\exp\left\{\frac{-(\Omega_s+\Omega_i)^2}{4\sigma_p^2}\right\}\mathrm{sinc}\left(\frac{\Delta \mathrm{kL}}{2}\right), \tag{23}$$

where $\Omega_{s(i)}$ is related to $\omega_{s(i)}$ and central frequency of signal (idler) field $\omega_{s0(i0)}$ through the relation $\Omega_{s(i)}=\omega_{s(i)}-\omega_{s0(i0)}$. Here the wave-vector mismatch term Δk, approximated by only

#250441 Received 18 Sep 2015; accepted 27 Oct 2015; published 2 Nov 2015

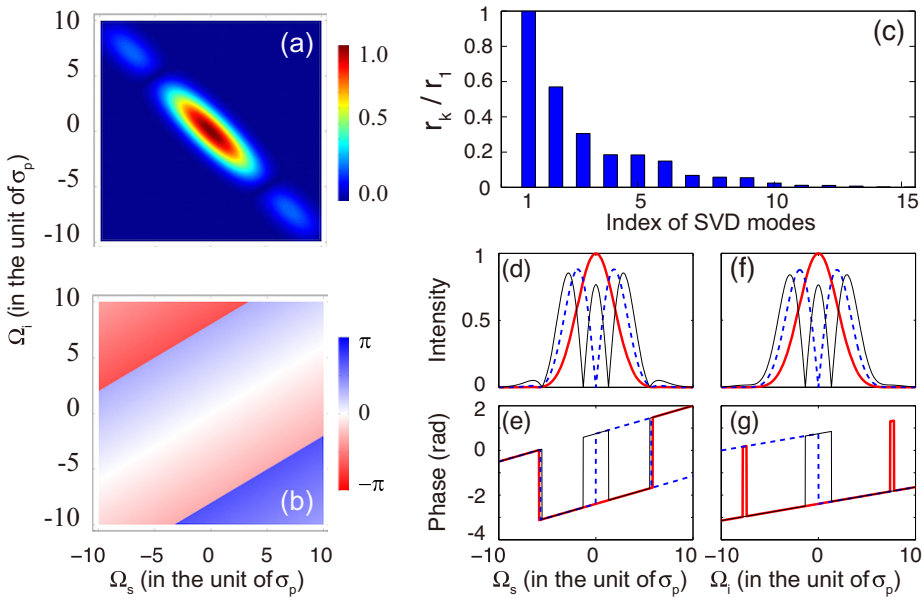

Fig. 2. Spectral properties of twin beams generated by a pulse pumped FOPA with broad gain bandwidth in telecom band. (a) Normalized absolute value and (b) phase of the JSF, $|F(\Omega_s,\Omega_i)/F(0,0)|$ and $\arctan(\frac{Re\{F(\Omega_s,\Omega_i)\}}{Im\{F(\Omega_s,\Omega_i)\}})$. (c) Relative mode strength r_k/r_1 for the decomposed k-th order temporal mode of twin beams $\phi_k(\omega_s)\psi_k(\omega_i)$. (d) The intensity and (e) phase of the first three decomposed mode in signal field $\phi_k(\Omega_s)$ $(k=1,2,3)$. (f) The intensity and (g) phase of the first three decomposed mode in idler field $\psi_k(\Omega_i)$ $(k=1,2,3)$. In plots (d)-(g), solid, dashed and dot-dashed lines are for the mode with index $k=1$, $k=2$, and $k=3$, respectively. In the calculation, we have $2\gamma P_p+\frac{\beta_2}{4}\Delta^2=0$, $\beta_2=0.2\times\frac{2\sigma_p}{L\Delta}$ and $\beta_3=0.2\times\frac{2\sigma_p}{L\Delta^2}$ in Eq. (24)

considering the 2nd-order and 3rd-order dispersion coefficients of the nonlinear fiber β_2 and β_3, is given by [26]

$$\Delta k \approx 2\gamma P_p+\frac{\beta_2}{4}\Delta^2+\frac{\beta_2}{2}\Delta(\Omega_s-\Omega_i)+\frac{\beta_3}{8}\Delta^2(\Omega_s+\Omega_i), \tag{24}$$

where $\Delta=\omega_{s0}-\omega_{i0}$ is the detuning between the signal and the idler fields. Note that, at the central frequency of the signal and idler fields $(\Omega_s,\Omega_i=0)$, the maximum gain is achieved when the first two terms in Eq. (24) counterbalance each other by satisfying the condition $2\gamma P_p+\frac{\beta_2}{4}\Delta^2=0$. So we will adapt this condition in the numerical analysis presented hereinafter.

We first study the temporal mode property of the twin beams by calculating the JSF. For the sake of brevity, all the frequency scales are in the unit of the pump bandwidth σ_p. In the calculation, the dispersion coefficients $\beta_2=0.2\times\frac{2\sigma_p}{L\Delta}$ and $\beta_3=0.2\times\frac{2\sigma_p}{L\Delta^2}$ are substituted in Eqs. (23) and (24). Figure 2(a) plot the normalized amplitude of JSF $|F(\Omega_s,\Omega_i)/F(0,0)|$. One sees that the frequencies of signal and idler fields are anti-correlated. The distribution ranges of frequency in the direction perpendicular and parallel to the line of $\Omega_s+\Omega_i=0$ are confined by the the pump envelope term $\exp(\frac{-(\Omega_s+\Omega_i)^2}{4\sigma_p^2})$ and phase matching term $\mathrm{sinc}(\frac{\Delta kL}{2})$, respectively. Figure 2(b) plots the phase of JSF, $\arctan(\frac{Re\{F(\Omega_s,\Omega_i)\}}{Im\{F(\Omega_s,\Omega_i)\}})$. One sees that the phase is within the range $[-\pi,\pi]$. The discontinuity of the phase values comes from the π phase jump, which is

#250441 Received 18 Sep 2015; accepted 27 Oct 2015; published 2 Nov 2015

occurred when the value of $\mathrm{sinc}[\frac{\Delta kL}{2}]$ changes from positive to negative or vice versa.

We then study the decomposed temporal modes of the signal and idler twin beams. In the simulation, the normalized amplitude and phase of the JSF in Figs. 2(a) and 2(b) are digitized with a 1000×1000 matrix $\bar{M}$, and the matrix is decomposed into the form $\bar{M} = \bar{S}\bar{\Lambda}\bar{I}$, where matrix $\bar{\Lambda}$ is diagonalized with the diagonal elements serving as the mode amplitudes r_k, and $\bar{S}$ ($\bar{I}$) is the matrix representing mode profiles $\phi_k(\Omega_s)$ ($\psi_k(\Omega_i)$ of the signal (idler) by the discrete relation $\bar{S}_{lk} = \phi_k(l = \Omega_s/\sigma_p)$ ($\bar{I}_{kl} = \psi_k(l = \Omega_i/\sigma_p)$). Figure 2(c) shows the relative mode strength r_k/r_1 for the decomposed mode with the index k. It is clear that the amplitudes of higher order modes attenuate quickly, therefore, for the signal and idler twin beams, most of the contribution is included in the modes with $k \leq 10$.

Figures 2(d) and 2(e) show the temporal mode profiles of individual signal beam $\phi_k(\Omega_s)$, in which only the first three dominant modes are plotted. From the mode intensity $|\phi_k(\Omega_s)|^2$ in Fig. 2(d), one sees that the spectral bandwidth of the mode increase with the mode index k, and the number of predominant peaks is the same as the mode index k, although the small peaks which are less than 10% of the predominant peaks may exist due to the oscillation of the phase matching term $\mathrm{sinc}(\frac{\Delta kL}{2})$. From the phase distribution $\mathrm{Arg}[\phi_k(\Omega_s)]$ in Fig. 2(e), one sees that the phase varies linearly except in some frequency points at which a π phase jump exists. Comparing Figs. 2(d) and 2(e), we find that the π phase jump happens at the frequencies at which the values of the intensity $|\phi_k(\Omega_s)|^2$ are zero.

The mode profiles of the intensity and phase distributions of individual idler beam, $\psi_k(\Omega_i)$ and $\mathrm{Arg}[\psi_k(\Omega_i)]$, are shown in Figs. 2(f) and 2(g), respectively. We find that the difference between the intensity distributions of signal ($|\phi_k(\Omega_s)|^2$) and idler ($|\psi_k(\Omega_i)|^2$) modes is very small. This is because the absolute value of the JSF in Fig. 2(a) is only slightly asymmetric with respect to the line of $\Omega_s + \Omega_i = 0$. On the contrary, the phase distribution of the $\psi_k(\Omega_i)$ in Fig. 2(g) differs significantly from that of $\phi_k(\Omega_s)$ in Fig. 2(e). The notable difference is in consistent with the phase distribution of the JSF in Fig. 2(b), where the asymmetry with respect to the line of $\Omega_s + \Omega_i = 0$ is more obvious than that in Fig. 2(a) because the dispersion for the signal and idler field is different.

3. Generation of continuous variable entanglement

After applying SVD to JSF (see Eq. (12)), the decomposed temporal modes of the signal and idler fields, defined by $\phi_k(\Omega_s)$ and $\psi_k(\Omega_i)$, respectively, are decoupled from each other. Therefore, we can study the CV entanglement of the signal and idler fields by utilizing the single-mode method [1].

According to the generalized operators of the kth order mode in Eqs. (19)-(22), the quadrature-phase amplitudes of signal (idler) field, $X_{ks(ki)}$ and $Y_{ks(ki)}$, are defined as

$$\hat{X}_{ks(ki)} = \frac{1}{\sqrt{2}}(\hat{B}_{ks(ki)} + \hat{B}^{\dagger}_{ks(ki)}) \tag{25}$$

$$\hat{Y}_{ks(ki)} = \frac{-i}{\sqrt{2}}(\hat{B}_{ks(ki)} - \hat{B}^{\dagger}_{ks(ki)}). \tag{26}$$

By substituting Eqs. (17)-(18) into Eqs. (25)-(26) and by assuming the input of the FOPA is in vacuum state, we obtain the quadrature variances of the signal (idler) field in the kth order mode $\langle \Delta\hat{X}^2_{s(i)} \rangle = \langle \hat{X}^2_{s(i)} \rangle - \langle \hat{X}_{s(i)} \rangle^2$ and $\langle \Delta\hat{Y}^2_{s(i)} \rangle = \langle \hat{Y}^2_{s(i)} \rangle - \langle \hat{Y}_{s(i)} \rangle^2$:

$$\langle \Delta\hat{X}^2_{s(i)} \rangle = \langle \Delta\hat{Y}^2_{s(i)} \rangle = \frac{\cosh^2(r_k G) + \sinh^2(r_k G)}{2}. \tag{27}$$

Subsequently, it is straightforward to deduce the variances of the correlated quadrature-phase

#250441 Received 18 Sep 2015; accepted 27 Oct 2015; published 2 Nov 2015

amplitudes of the twin beams, $\langle\Delta(\hat{X}_s-\hat{X}_i)^2\rangle$ and $\langle\Delta(\hat{Y}_s+\hat{Y}_i)^2\rangle$:

$$\langle\Delta(\hat{X}_{ks}-\hat{X}_{ki})^2\rangle=\langle\Delta(\hat{Y}_{ks}+\hat{Y}_{ki})^2\rangle=\frac{1}{[\cosh(r_kG)+\sinh(r_kG)]^2}. \tag{28}$$

Substituting Eq. (28) into the inseparability coefficient $I_k=\langle\Delta(\hat{X}_{ks}-\hat{X}_{ki})^2\rangle+\langle\Delta(\hat{Y}_{ks}+\hat{Y}_{ki})^2\rangle<2$ [27], we have

$$I_k=\frac{2}{[\cosh(r_kG)+\sinh(r_kG)]^2}<2, \tag{29}$$

which indicates that for signal and idler beams, described by the pair of mode functions $\phi_k(\omega_s)$ and $\psi_k(\omega_i)$, the Duan's inseparability criterion of entanglement is satisfied [27]. Equation (29) clearly shows that I_k always decreases with the gain coefficient G and trends to zero as G approaches to infinity. However, for a fixed coefficient G, the value of I_k increases with the mode index k because the mode amplitude r_k decreases with the increase of k. It is worth noting that if the JSF of the FOPA is spectrally factorable, i.e., $F(\omega_s,\omega_i)=\phi(\omega_s)\psi(\omega_i)$, we have $r_k=\delta_{k,1}$. In this case, only the fundamental mode exists, and I_k in Eq. (29) is the same as that in Ref. [21], describing a CW pumped FOPA operated as a single mode parametric amplifier.

4. Detection of quadrature entanglement

Having demonstrated that the entangled signal and idler twin beams can be decomposed into many pairs of SVD modes, in this section, we will formulate a homodyne detection (HD) process and analyze how to improve the measured degree of entanglement. For simplicity, we assume the polarization states of the individual signal (idler) field and its local oscillator of the HDs (HDi), LOs (LOi), are identical. So the optical fields can be represented as scalars.

The principle of measuring the quadrature components of signal and idler field by using homodyne detectors, HDs and HDi, is shown in the area framed by the dash-dotted line in Fig. 1. The HDs/HDi is comprised of a 50/50 beam splitter (BS) and two photodiodes (PD). Because the signal and idler twin beams are pulsed fields, we take the local oscillators, LOs and LOi, as transform-limited pulses in the form of

$$E_{Ls(Li)}(t)=|\alpha_{Ls(Li)}|e^{i\theta_{Ls(i)}}\int A_{Ls(Li)}(\omega)e^{-i\omega t}d\omega+c.c., \tag{30}$$

where the amplitude of LOs (LOi) is much higher than that of the signal (idler) field, i.e., $|\alpha_{Ls(Li)}|>>1$, $\theta_{Ls(i)}$ represents the phase of LOs (LOi), and $A_{Ls(Li)}(\omega)$ is the spectrum of LOs (LOi) satisfying the normalization condition $\int|A_{Ls(Li)}(\omega)|^2d\omega=1$. The overall efficiency of the HDs (HDi), including the transmission efficiency of the optical paths and the quantum efficiency of the photodiodes, is denoted by $\eta_{s(i)}$, and can be modeled by a beam splitter with transmission efficiency $\eta_{s(i)}$. In this case, the detected field operators of individual signal and idler beams, $\hat{c}_s(\omega_s)$ and $\hat{c}_i(\omega_i)$, are written as

$$\hat{c}_s(\omega_s)=\sqrt{\eta_s}\hat{b}_s(\omega_s)+i\sqrt{1-\eta_s}\hat{v}_s(\omega_s) \tag{31}$$

$$\hat{c}_i(\omega_i)=\sqrt{\eta_i}\hat{b}_i(\omega_i)+i\sqrt{1-\eta_i}\hat{v}_i(\omega_i), \tag{32}$$

where $\hat{v}_s(\omega_s)$ and $\hat{v}_i(\omega_i)$ are vacuum operators introduced by the optical losses.

When the response times of the HDs and HDi are much longer than the pulse durations of signal, idler, LOs, and LOi fields, the result of the homodyne detection can be treated as a time integral of the optical fields. The photocurrent out of HDs and HDi are expressed as [28]:

$$\hat{i}_{s(i)}=q\int_{-\infty}^{\infty}[E_{Ls(Li)}\hat{E}'^{(-)}_{s(i)}+h.c.]dt, \tag{33}$$

#250441 Received 18 Sep 2015; accepted 27 Oct 2015; published 2 Nov 2015

where

$$\hat{E}'^{(-)}_{s(i)} = \frac{1}{\sqrt{2\pi}} \int \hat{c}_{s(i)}(\omega) e^{-i\omega t} d\omega. \tag{34}$$

is the field operator of the detected signal (idler) beam, and the coefficient g is proportional to the electrical gain of detectors.

Since the decomposed modes functions, $\phi_k(\omega_s)$ and $\psi_k(\omega_i)$, form a complete and orthogonal set in the frequency domain of signal and idler beams, the spectra of LOs and LOi (see Eq. (30)) can be expanded into the Fourier series:

$$A_{Ls}(\omega_s) = \sum_k \xi_{ks} \phi_k(\omega_s) \tag{35a}$$

$$A_{Li}(\omega_i) = \sum_k \xi_{ki} \psi_k(\omega_i), \tag{35b}$$

with

$$\xi_{ks} = |\xi_{ks}| e^{-i\theta_{ks}} = \int_S A_{Ls}(\omega_s) \phi_k^*(\omega_s) d\omega_s \tag{36a}$$

$$\xi_{ki} = |\xi_{ki}| e^{-i\theta_{ki}} = \int_I A_{Li}(\omega_i) \psi_k^*(\omega_i) d\omega_i, \tag{36b}$$

where the complex coefficient ξ_{ks} (ξ_{ki}) characterizes the mode matching, $|\xi_{ks}|^2$ ($|\xi_{ki}|^2$) can be viewed as the mode-matching efficiency, and θ_{ks} (θ_{ki}) can be viewed as the relative phase between the kth order signal (idler) mode $\phi_k(\omega_s)$ ($\psi_k(\omega_i)$) and LOs (LOi). Using Eqs. (30) and (35), the photocurrents in Eq. (33) can be rewritten as

$$\hat{i}_s = q|\alpha_{Ls}| \sum_k |\xi_{ks}| [\sqrt{\eta_s} \hat{X}_{ks}(\theta_s) + \sqrt{1-\eta_s} \hat{X}_v] \tag{37a}$$

$$\hat{i}_i = q|\alpha_{Li}| \sum_k |\xi_{ki}| [\sqrt{\eta_i} \hat{X}_{ki}(\theta_i) + \sqrt{1-\eta_i} \hat{X}_v], \tag{37b}$$

where

$$\hat{X}_{ks(ki)}(\theta_{s(i)}) = \frac{1}{\sqrt{2}} (e^{-i\theta_{s(i)}} \hat{B}_{ks(ki)} + e^{i\theta_{s(i)}} \hat{B}^\dagger_{ks(ki)}). \tag{38}$$

with $\theta_{s(i)} = \theta_{Ls(i)} + \theta_{ks(i)}$ denoting the phase angle of the quadrature component of kth order signal (idler) mode, and $\hat{X}_v$ is the quadrature operator of the vacuum field. For the case of $\theta_s = \theta_i = 0$ and $\theta_s = \theta_i = \pi/2$, respectively, $\hat{X}_{ks(ki)}(\theta_{s(i)})$ corresponds to the quadrature amplitude and quadrature phase defined in Eq. (25). Note that in order to clearly demonstrate the mode mismatching effect on measured degree of entanglement, in the analysis hereinafter, we will assume the transmission efficiency of twin beams and detection efficiency of detectors are ideal, i.e., $\eta_s = \eta_i = 1$.

4.1. The spectrum of the LO is matched to a specified SVD mode

When the spectra of LOs and LOi are the same as a pair of decomposed temporal mode, say the kth order modes, Eq. (35) is simplified as

$$A_{Ls}(\omega_s) = \phi_k(\omega_s) \tag{39a}$$

$$A_{Li}(\omega_i) = \psi_k(\omega_i), \tag{39b}$$

and the general expression of the complex coefficients in Eq. (36) becomes $\xi_{sk} = \xi_{ik} = 1$ and $\xi_{sl} = \xi_{il} = 0$ ($l \neq k$) because of the orthogonality. In this case, only the signal and idler fields

#250441 Received 18 Sep 2015; accepted 27 Oct 2015; published 2 Nov 2015

described by the mode functions $\phi_k(\omega_s)$ and $\psi_k(\omega_i)$, respectively, will contribute to the photocurrents in Eq. (37). The evolution of the detected signal and idler fields is described by Eqs. (17) and (18) with an effective gain of $G_{eff} = r_k G$, and the measured inseparability I_k is given by Eq. (29), which goes to zero as G becomes infinitely large.

Among the decomposed SVD modes, the fundamental mode ($k = 1$) has the largest mode amplitude r_1, so its effective parametric gain $G_{eff} = r_1 G$ is the highest. Hence, we can obtain the highest degree of entanglement when the spectra of LOs and LOi are shaped to satisfy the conditions $A_{Ls}(\omega_s) = \phi_1(\omega_s)$ and $A_{Li}(\omega_i) = \psi_1(\omega_i)$. In particular, when the JSF of the FOPA is factorable, i.e., $F(\omega_s, \omega_i) = \phi(\omega_s)\psi(\omega_i)$, and the spectra of LOs and LOi satisfy the conditions $A_{Ls}(\omega_s) = \phi(\omega_s)$ and $A_{Li}(\omega_i) = \psi(\omega_i)$, we will obtain the maximum degree of entanglement for a given gain parameter G because $r_1 = 1$ and $r_k = 0$ $(k \neq 1)$, which means all the energy of twin beams is concentrated in the fundamental mode. However, it is worth pointing out that the factorable JSF is not a necessary condition for obtaining the entanglement with a high degree. As we have seen, we can always obtain the high quality entanglement characterized by inseparability $I_k \to 0$ as $G \to \infty$ by shaping the spectrum of LOs and LOi to a pair of decomposed modes and by increasing the gain coefficient G.

4.2. *The spectrum of the LO is not matched to any particular SVD mode*

In general, the LOs and LOi are not matched to any pair of the decomposed modes. The photocurrent out of HDs/HDi is contributed by all the temporal modes non-orthogonal to the spectrum of LOs/LOi (the mode-matching efficiency $|\xi_{ks}|^2 \neq 0/|\xi_{ki}|^2 \neq 0$, see Eq. (37)). Now let us analyze how the multi-mode nature of the twin beams affect the experimentally measured inseparability

$$I_{exp} = \langle \Delta \hat{X}_-^2 \rangle_{exp} + \langle \Delta \hat{Y}_+^2 \rangle_{exp}, \tag{40}$$

with

$$\langle \Delta \hat{X}_-^2 \rangle_{exp} = \frac{\langle \Delta(\hat{i}_s - \hat{i}_i)^2 \rangle}{q^2 |\alpha_{Ls}||\alpha_{Li}|} \Big\|_{\theta} \tag{41a}$$

$$\langle \Delta \hat{Y}_+^2 \rangle_{exp} = \frac{\langle \Delta(\hat{i}_s + \hat{i}_i)^2 \rangle}{q^2 |\alpha_{Ls}||\alpha_{Li}|} \Big\|_{\theta+\frac{\pi}{2}} \tag{41b}$$

denoting the measured variances of the correlation of quadrature-phase amplitudes of twin beams, where $\theta = \theta_{Ls} = \theta_{Li}$ refers to the phase of local oscillators. According to the expression of photocurrent in Eq. (37), we have

$$\langle \Delta \hat{X}_-^2 \rangle_{exp} = V_{Xs} + V_{Xi} - 2C_X \tag{42a}$$

$$\langle \Delta \hat{Y}_+^2 \rangle_{exp} = V_{Ys} + V_{Yi} + 2C_Y, \tag{42b}$$

with

$$V_{Xs} = V_{Ys} = \sum_{k=1}^{\infty} |\xi_{ks}|^2 [\cosh^2(r_k \times G) + \sinh^2(r_k \times G)]/2 \tag{43a}$$

$$V_{Xi} = V_{Yi} = \sum_{k=1}^{\infty} |\xi_{ki}|^2 [\cosh^2(r_k \times G) + \sinh^2(r_k \times G)]/2, \tag{43b}$$

and

$$C_X = \sum_{k=1}^{\infty} C_{Xk} = \sum_{k=1}^{\infty} |\xi_{ks}\xi_{ki}| \cosh(r_k \times G) \sinh(r_k \times G) \cos(\theta_{Ls} + \theta_{Li} + \theta_{ks} + \theta_{ki}), \tag{44a}$$

$$C_Y = \sum_{k=1}^{\infty} C_{Yk} = -\sum_{k=1}^{\infty} |\xi_{ks}\xi_{ki}| \cosh(r_k \times G) \sinh(r_k \times G) \cos(\theta_{Ls} + \theta_{Li} + \theta_{ks} + \theta_{ki}). \tag{44b}$$

#250441 Received 18 Sep 2015; accepted 27 Oct 2015; published 2 Nov 2015

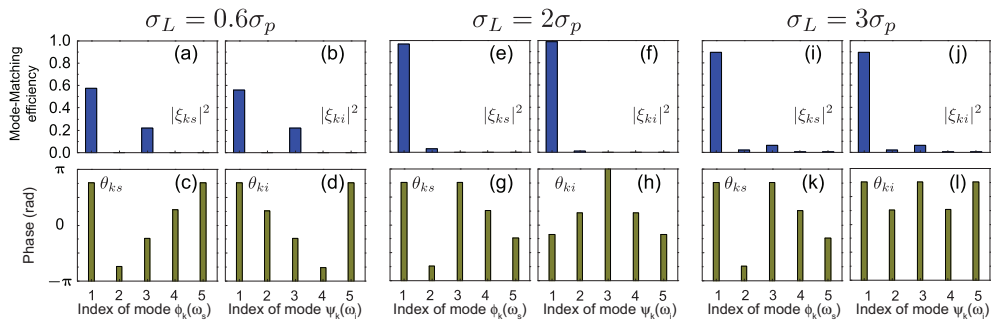

Fig. 3. Mode matching efficiency $|\xi_{ks}|^2$ ($|\xi_{ki}|^2$) and phase θ_{ks} (θ_{ki}) for the kth order decomposed signal (idler) mode $\phi_k(\omega_s)$ ($\psi_k(\omega_i)$) when the bandwidths of LOs and LOi are $\sigma_L = 0.6\sigma_p$ (plots (a)-(d)), $\sigma_L = 2\sigma_p$ (plots (e)-(h)), and $\sigma_L = 3\sigma_p$ (plots (i)-(l)), respectively. The parameters of the FOPA are the same as those in Fig.2

where $V_{Xs(i)}$ and $V_{Ys(i)}$ are the phase-independent noise variances for the signal (idler) field, and C_X and C_Y, which are sensitive to phase between the local oscillators and the signal and idler modes, respectively, are the correlation terms of the quadrature-phase amplitudes between the signal and the idler beams, respectively. Note that the minus sign in Eq. (44b) is originated from the $\pi/2$-phase difference between two quadrature components.

From Eqs. (40)-(44), one sees that the key to minimize the inseparability I_{exp} is to maximize the correlation terms in Eqs. (44a) and (44b) by adjusting the phase of the local oscillators θ_{Ls} and θ_{Li}. It is straightforward to maximize the individual terms C_{Xk} and C_{Yk} for a given mode index k in Eqs. (44a) and (44b), however, it is difficult to maximize the correlation term for all the terms with $|\xi_{ks}|^2 \neq 0/|\xi_{ki}|^2 \neq 0$, because the phase θ_{ks} and θ_{ki} may varies with the mode index k. This will generally result in a decrease in the measured degree of entanglement.

Having understood the measurement principle of entanglement, we are ready to study the parameters that will influence the degree of the measured quadrature amplitude entanglement generated by the FOPA analyzed in Sec. 2.3, which has a broad gain bandwidth in telecom band. Assuming the local oscillators LOs and LOi have the same bandwidth σ_L, but their central frequencies are the same as the corresponding signal and idler fields, the spectrum of LOs/LOi, which is Gaussian shaped and transform limited, can be expressed as:

$$A_{Ls(Li)}(\omega_{s(i)}) = \frac{1}{\sqrt{\pi^{1/2}\sigma_L}} \exp\{\frac{-(\omega_{s(i)} - \omega_{s0(i0)})^2}{2\sigma_L^2}\}. \tag{45}$$

We first analyze the mode matching of the homodyne detection systems. Using the twin beams with mode structure shown in Fig. 2 and substituting Eq. (45) into Eq. (36), we calculate the mode matching coefficient for each pair of the decomposed SVD modes. Figure 3 shows the calculated mode-matching efficiency and the phase for the kth order decomposed signal/idler mode $\phi_k(\omega_s)/\psi_k(\omega_i)$ when the bandwidths of LOs and LOi are $\sigma_L = 0.6\sigma_p$, $\sigma_L = 2\sigma_p$, and $\sigma_L = 3\sigma_p$, respectively. For each case, one sees that the phase $\theta_{ks(i)}$ of the signal (idler) mode varies with the index k, indicating that it is impossible to simultaneously obtain the maximized correlation terms C_{Xk} and C_{Yk} for each pair of decomposed modes. On the other hand, since only the modes with the non-zero mode matching efficiencies contribute to the measurement of HDs and HDi, Fig. 3 shows that the main contribution is from the modes with index number $k < 5$. Moreover, for the mode with a fixed index number, the mode matching coefficient varies with the bandwidth σ_L. For the case of $\sigma_L = 0.6\sigma_p$ (Figs. 3(a)-(d)), the sum of mode-matching efficiency for the first- and third-order modes are about 90%, and the mode matching efficiency

#250441 Received 18 Sep 2015; accepted 27 Oct 2015; published 2 Nov 2015

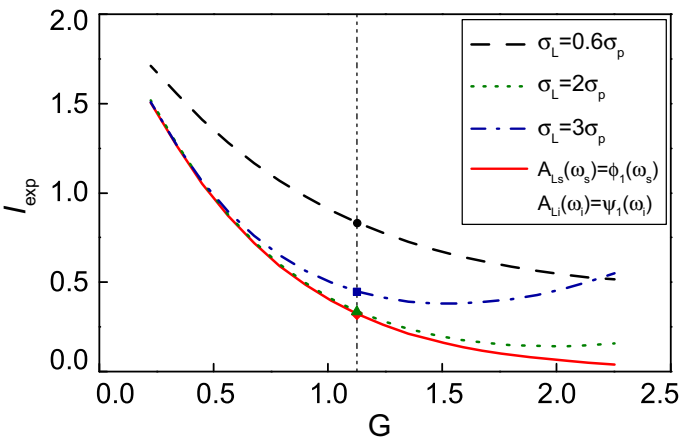

Fig. 4. Measured inseparability of twin beams, I_{exp}, as a function of gain coefficient G when the bandwidths of LOs and LOi are $\sigma_L = 0.6\sigma_p$, $\sigma_L = 2\sigma_p$ and $\sigma_L = 3\sigma_p$, respectively. As a comparison, I_{exp}=I_1 for the LOs and LOi with the spectra the same as the fundamental modes $\phi_1(\omega_s)$ and $\psi_1(\omega_i)$ is also plotted. The results obtained for the JSF in Fig. 2 are marked by cross points between the data and dashed line.

for the other modes are too small to be obviously observed; for the case of $\sigma_L = 3\sigma_p$ (Figs. 3(i)-(l)), the mode matching efficiency for the first order is about 90%. While for the case of $\sigma_L = 2\sigma_p$ (Figs. 3(e)-(h)), the mode matching is obviously better than the other two cases because the mode-matching efficiency for the first order mode is very close to 1.

We then study the dependence of the measured degree of entanglement upon the mode matching of HDs and HDi by numerically calculating the inseparability I_{exp} in different conditions. Figure 4 shows the calculated I_{exp} as a function of the gain coefficient G when the bandwidths of LOs and LOi are $\sigma_L = 0.6\sigma_p$, $\sigma_L = 2\sigma_p$, and $\sigma_L = 3\sigma_p$, respectively. In the calculation, for each gain coefficient, we deduce the corresponding mode structure and mode matching for different spectrum of LOs and LOi, which is similar to the procedure of obtaining the plots in Figs. 2 and 3. The results corresponding to the JSF in Fig. 2 are marked by cross points between the data and the dashed line. Additionally, as a comparison, the inseparability I_1 for LOs and LOi with the spectra the same as the corresponding fundamental modes $\phi_1(\omega_s)$ and $\psi_1(\omega_i)$ is also plotted in Fig. 4 as a function of G. Obviously, for a fixed gain coefficient G, the value of I_1 is always smaller than that of I_{exp}.

In Fig. 4, when the spectra of LOs and LOi are not matched to the fundamental modes, one sees that for a fixed value of G, the lowest and highest I_{exp} respectively correspond to the case of $\sigma_L = 2\sigma_p$ and $\sigma_L = 0.6\sigma_p$. If we compare the mode matching efficiency in Fig. 3, it is straightforward to see that the measured degree of entanglement increase with the mode matching efficiency between the local oscillators and the fundamental modes, $|\xi_{1s}|^2$ and $|\xi_{1i}|^2$, and the departure between I_{exp} and I_1 will increase when the spectra of LOs and LOi are more evenly distributed among the decomposed othogonal modes.

From Fig. 4, one also sees that different from I_1, which always decreases with the increase of G, the measured I_{exp} may increase with G when G is larger than a certain value. For the case of $\sigma_L = 3\sigma_p$, it is obvious that I_{exp} start to increase with G for $G > 1.4$. For the case of $\sigma_L = 2\sigma_p$, this kind variation trend is also observable: I_{exp} increases with G for $G > 1.9$. We think the reason is because the the correlation term C_{Xk}/C_{Yk} (see Eqs. (44a) and (44b)) for different k can not simultaneously achieve the maximum for the LOs/LOi with a given phase. Although the mode matching efficiency of the first order mode is the highest (see Fig. 3), the

#250441 Received 18 Sep 2015; accepted 27 Oct 2015; published 2 Nov 2015

noise variance of I_{exp} contributed by the signal and idler beams in higher order SVD modes may exponentially increase with G, which will results in the unusual trend of I_{exp}. Moreover, it is worth noting that the influence of mode mismatching effect on measured entanglement is not equivalent to an effective detection loss because the noise contributed by higher order modes with $|\xi_{ks}|^2 \neq 0/|\xi_{ki}|^2 \neq 0$ will become significant, particularly in the high gain regime of FOPA.

5. Conclusion

In summary, we theoretically analyzed the temporal mode structure and the degree of measured CV entanglement of the twin beams generated from a pulse-pumped FOPA by applying the SVD to the JSF. We are able to successfully decouple different temporal modes and derive the input-output relation for each temporal mode. The results indicate that the temporal mode structures are highly sensitive to the dispersion of the nonlinear fiber and the gain coefficient of FOPA. While for the measurement of CV entanglement, when the temporal modes of LOs and LOi are the same as one pair of decomposed modes, $\phi_k(\omega_s)$ and $\psi_k(\omega_i)$, the measurement result of the homodyne detection systems is only contributed by the signal and idler fields in the modes $\phi_k(\omega_s)$ and $\psi_k(\omega_i)$, which is similar to case of pulsed pumped parametric amplifier having a factorizable JSF; when the modes of LOs and LOi can not match any pair of the decomposed modes, the measurement result of the homodyne detection systems is contributed by all the modes non-orthogonal to the spectra of local oscillators, leading to a poor value of the inseparability. Therefore, in order to obtain the high degree CV entanglement, making the JSF factorable is not necessary, but matching the spectra of local oscillators to one pair of decomposed modes is crucial. Moreover, for the FOPA with broad gain bandwidth of FWM in telecome band, we numerically studied the temporal mode functions of the twin beams, and calculated its corresponding degree of CV entanglement when the spectra of LOs and LOi of HD systems are varied. The results demonstrate the detailed temporal mode structure of this kind of FOPA as well as the strategy for optimizing the spectra of the local oscillators in the detection process. Hence, our study is useful for developing a high-quality source of pulsed CV entanglement by using the FOPA.

Our investigation indicates that the determination of the JSF, including the absolute value ($|F(\omega_s', \omega_i')|$) and the phase term $\arctan(\frac{Re\{F(\Omega_s,\Omega_i)\}}{Im\{F(\Omega_s,\Omega_i)\}})$, is utmost important for the mode analysis of a pulse-pumped parametric process. So far, the measurements of the absolute value of JSF have been demonstrated [29–32]. If there is a practical scheme to realize the measurement of the phase term of JSF, which has not been reported yet, it will be straightforward to realize the required mode matching by shaping the spectra of LOs and LOi [33].

Acknowledgment

This work was supported in part by the National NSF of China (No. 11527808, No. 11304222), the State Key Development Program for Basic Research of China (No. 2014CB340103), the Specialized Research Fund for the Doctoral Program of Higher Education of China (No. 20120032110055), PCSIRT and 111 Project B07014.